



# Study on the numerical simulation of laying powder for the selective laser melting process

Liu Cao<sup>1</sup>

Received: 28 March 2019 / Accepted: 20 September 2019  
© Springer-Verlag London Ltd., part of Springer Nature 2019

## Abstract

Because the selective laser melting (SLM) formation process involves rapid melting and solidification of slices, the SLM process places high demands on the tightness, uniformity, and flatness of the powder layer. Based on the discrete element method (particle contact force model, particle collision judgment algorithm, and particle motion equation) and the SLM laying powder process, a numerical simulation of the SLM laying powder process was carried out. For the performance measurement experiment of the TC4 titanium alloy powder, the powder bulk density, tap density, and angle of repose were calculated and analyzed. It was found that the tap density increased by 7.5% compared to the bulk density, and the calculated average angle of repose ( $32.6^\circ$ ) was in good agreement with the experimental data ( $33.2^\circ$ ), thus verifying the accuracy of the calculation model used for the SLM laying powder. The influences of different scraping methods and scraping speeds on the quality of the laying powder were calculated and analyzed. It was found that the scraping method using a roller (not rotating) obtained the highest tightness and most uniform powder distribution, and, as the scraping speed increased, the laying tightness tended to decrease linearly. The results of the numerical simulation study of the SLM laying powder process can be used to guide the actual SLM laying powder process and, alternatively, provide basic data for the numerical simulation of SLM molten pool dynamics based on the particle scale.

**Keywords** Laying powder · Selective laser melting · Discrete element method · Tightness · Numerical simulation · Additive manufacturing

## Abbreviations

$m_e$	Equivalent mass of particle $i$ and particle $j$
$\mathbf{u}_n, \mathbf{u}_t$	Normal and tangential relative displacements of the particles, respectively
$t$	Time
$D_n, D_t$	Normal and tangential damping coefficients of the contact model, respectively
$E_n, E_t$	Normal and tangential elastic coefficients of the contact model, respectively
$\mathbf{F}_n, \mathbf{F}_t$	Normal and tangential components of the particle contact force, respectively

$I_e$	Equivalent moment of inertia of the particle
$\theta$	Rotation angle of the particle itself
$r$	Radius of rotation
$\mathbf{M}$	External torque of the particles
$\mu$	Coefficient of friction of the particles
$\text{sgn}$	A symbolic function
$\tilde{P}$	Created box for the particle $P$
$L_{ij}$	Spherical center distance between particle $i$ and particle $j$
$r_i, r_j$	Radius of particle $i$ and particle $j$ , respectively
$m_i$	Mass of particle $i$
$\ddot{\mathbf{u}}_i$	Acceleration of particle $i$
$\mathbf{F}_{sum}$	External force of the particle $i$ at the centroid
$I_i$	Moment of inertia of particle $i$
$\dot{\theta}_i$	Angular acceleration of particle $i$
$\mathbf{M}_{sum}$	External moment of the particle $i$ at the centroid
$(\dot{\mathbf{u}}_i)_N$	Particle velocity of the next time step
$(\dot{\theta}_i)_N$	Angular velocity of the next time step
$\Delta t$	Time step

✉ Liu Cao  
caoliu@gzhu.edu.cn

<sup>1</sup> Advanced Institute of Engineering Science for Intelligent Manufacturing, Guangzhou University, Guangzhou 510006, Guangdong, China

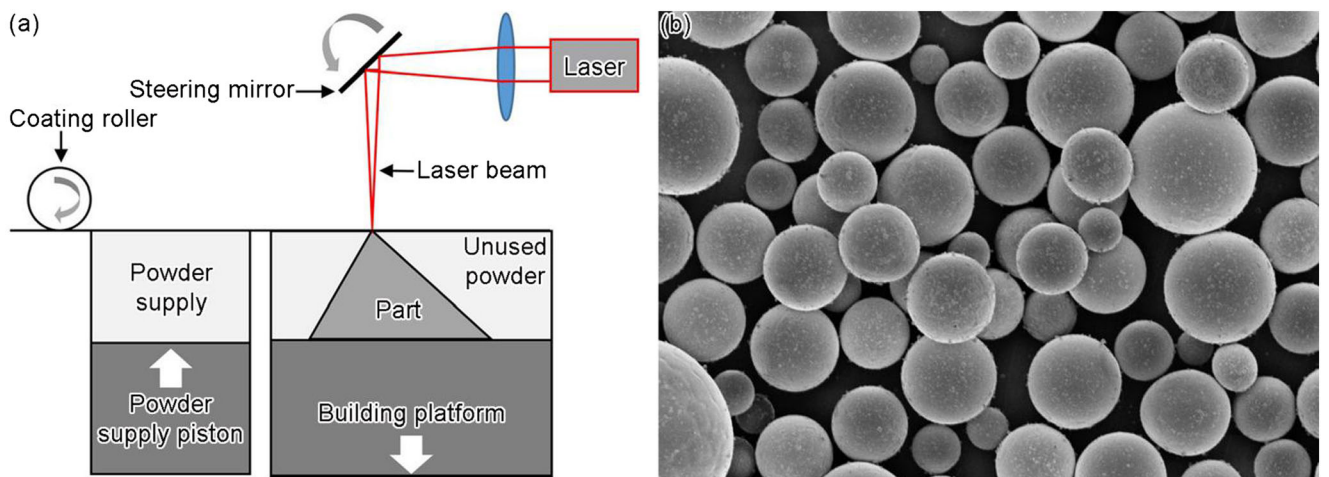


**Fig. 1** SLM technology and metal powder: **a** SLM schematic, and **b** metal particle morphology

## 1 Introduction

Based on the idea of “layer by layer” formation, additive manufacturing technology can directly and digitally

manufacture digital models into three-dimensional solid parts with high flexibility and no restrictions on the part’s structure [1]. Selective laser melting (SLM), as one of the additive manufacturing technologies for directly forming complex

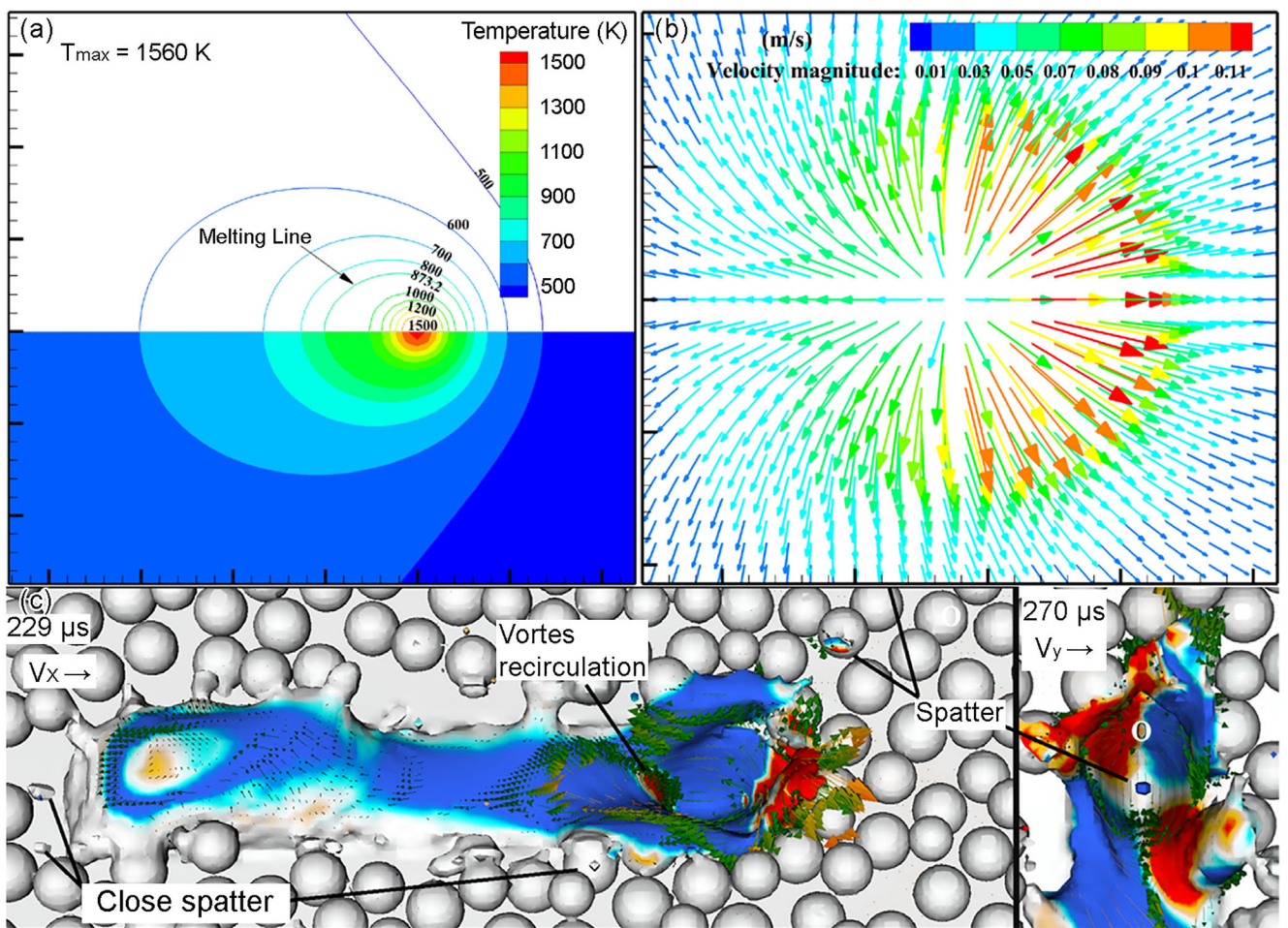


**Fig. 2** Numerical simulation of the dynamic behavior of an SLM molten pool: **a, b** based on the workpiece scale [14], and **c** based on the particle scale [15]

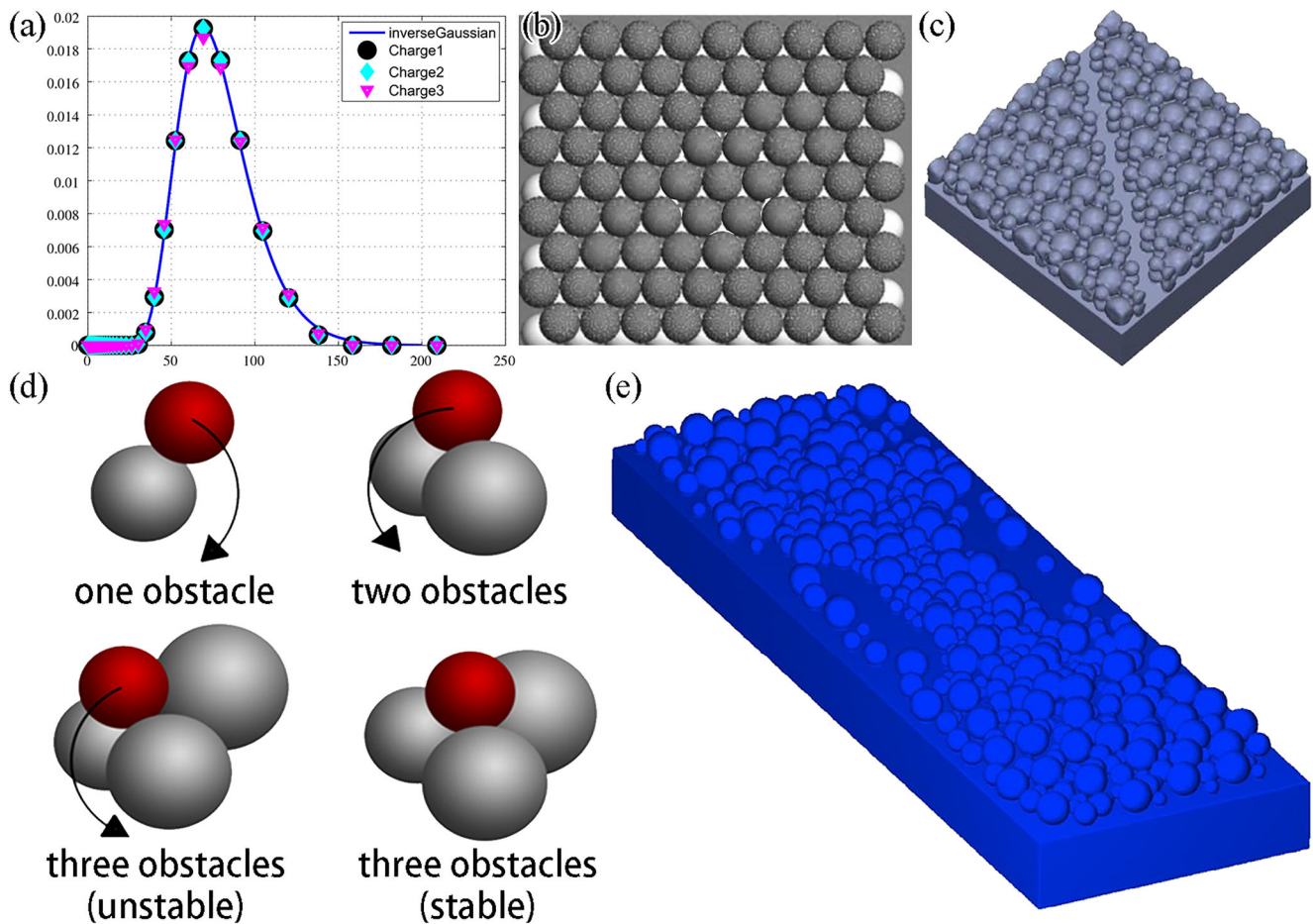


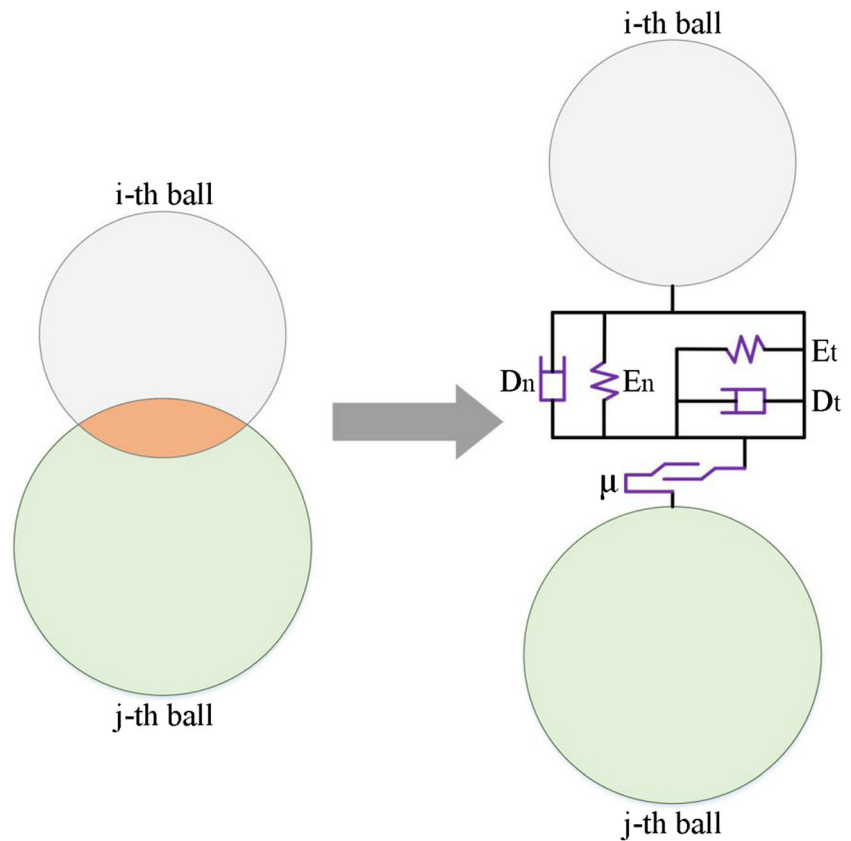
**Fig. 3** Particle size and laying distribution: **a** experimental determination of the particle size distribution (Gaussian fitting); **b** regular distribution under uniform size; **c** regular distribution under bipolar distribution; **d** raindrop model; and **e** discrete element method

metal parts, has been demonstrated in aerospace, automotive, medical, and other fields [2] (Fig. 1a). Since the formation process involves changes in the state of rapid melting and solidification of the slice, the SLM process has high demands for metallurgical quality and performance of the applied material. On the one hand, the metal powder raw material is required to have high sphericity, good fluidity, and narrow particle size distribution, and on the other hand, the powder coating should have good flatness, uniformity, and tightness [3, 4] (Fig. 1b).

Numerical simulation technology has been widely used in industrial production for its perceptibility and forward-thinking, and has become an effective technical means for studying physical processes and controlling defects in mechanical manufacturing [5, 6]. In the past 10 years, numerical simulation studies on the SLM formation process have gradually emerged, and these theoretical research works can be roughly divided into two directions: based on the workpiece scale [7–9], and based on the particle scale [10–12]. The so-called workpiece scale refers to the powder layer (including metal particles and pores) as a special material, indirectly describing

the temperature and flow field evolution in the SLM formation process by setting equivalent physical parameters and flow behavior models (Fig. 2a, b). Gusarov et al. [13] proposed the use of equivalent thermal conductivity to characterize the thermal conduction of the powder layer. The equivalent radiation heat transfer model was used to calculate the heating effect of the laser beam on the powder layer, and the influence of the laser beam mode on the SLM process was studied. Yuan et al. [14] carried out the numerical simulation of the SLM process based on Fluent, analyzed the internal flow of the molten pool caused by the Marangoni effect, and compared the influence of different process parameters on the size of the molten pool. This kind of simulation method can describe the temperature, flow, and stress field evolution in the SLM process by equivalent processing methods, but cannot describe the SLM formation process intuitively, and the accuracy depends mainly on the rationality of the equivalent processing models. The so-called particle scale refers to modeling based on the actual particle morphology, directly calculating the heating and melting effects of the laser on the metal particles and then describing the complex flow behavior of the metal

**Fig. 4** Schematic of the soft ball model



liquid between the particles (Fig. 2c). Khairallah et al. [15] used the multi-physics code ALE3D to study the dynamic behavior of an SLM molten pool based on the particle scale and directly calculated the distribution of pore defects at different scanning speeds. Panwisawas et al. [16] compared the effects of different lamination thicknesses on the formation effect, based on the open-source computational fluid

dynamics (CFD) code OpenFOAM. This kind of simulation method can directly describe the SLM formation process and directly predict the formation and evolution of defects such as pore and ball, but the premise is to obtain a reasonable particle size and laying distribution.

Numerical simulations of laying powder include particle size and laying distributions. Methods for obtaining particle

**Fig. 5** Schematic of the collision judgment

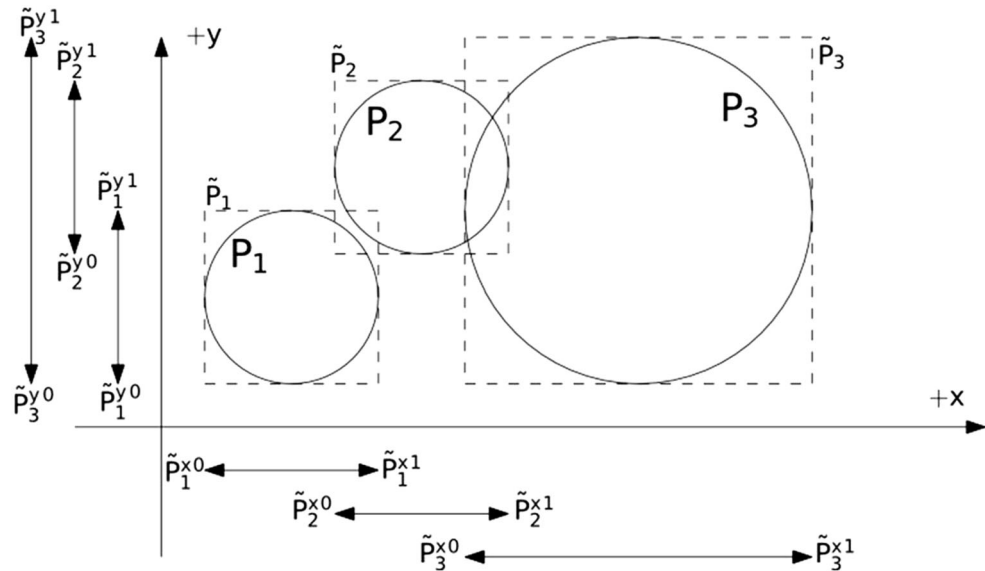
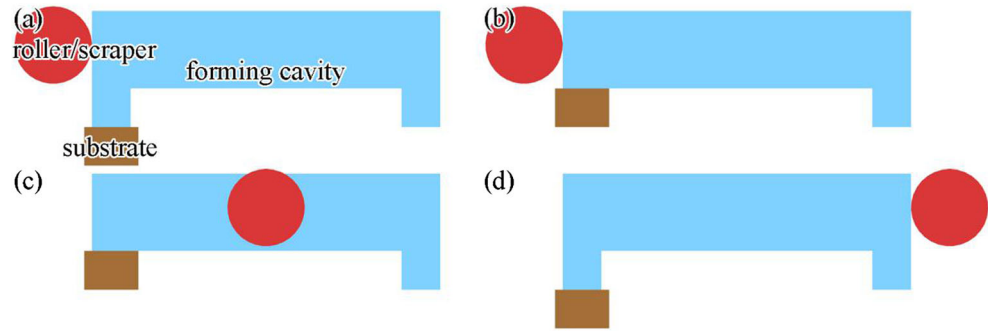


**Fig. 6** Schematic of the SLM laying powder process: **a** start; **b** substrate pushes out powder; **c** roller or scraper lays powder; and **d** finish



size distribution include artificial designation and experimental determination. The types of artificial designation [17] are divided into uniform size (single particle diameter), bipolar distribution (two particle diameters), normal distribution (particle diameter that satisfies the law of normal distribution), etc. Experimental determination [18] refers to the experimental measurement of the particle diameter, using statistical methods to obtain the actual particle diameter distribution curve, and using a correlation function (such as normal distribution) to fit the curve (Fig. 3a). It is clear that a more reasonable particle size distribution can be obtained by an experimental method. The purpose of the laying distribution is to obtain the particle locations, and the calculation methods include regular distribution [19], raindrop model (RDM) [20], and discrete element method (DEM) [21, 22]. The regular distribution requires artificially designated particle locations (Fig. 3b shows the regular distribution under uniform size, and Fig. 3c shows the regular distribution under a bipolar distribution). The core idea of placing new particles in RDM is to first anchor the existing particles in the vertical direction and then rotate to the equilibrium position (Fig. 3d). The core idea of DEM is to use a single particle as the calculation object, considering the normal contact and tangential contact between the particles, and the forces between the particles and the roller to obtain the laying distribution (Fig. 3e). In comparison, the regular distribution only truly reflects the actual particle distribution for simplified calculation scenarios. The implementation algorithm of RDM is simple, but it is difficult to control the tightness (particles account for the volume percentage of the entire powder layer, which is also called packing fraction), and it is often necessary

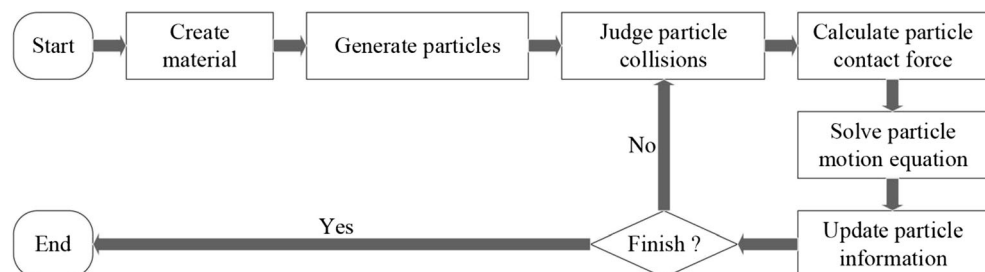
to artificially remove or add particles to obtain reasonable tightness. DEM can obtain a laying distribution that is basically in line with the actual situation, but its implementation algorithm is more complicated.

Based on the discrete element method (particle contact force model, particle collision judgment algorithm, and particle motion equation) and the SLM laying powder process, a numerical simulation of the SLM laying powder process was carried out. In order to verify the accuracy of the SLM laying powder calculation model, the powder bulk density, tap density, and angle of repose were calculated and compared with the experimental results of the performance measurement experiment of TC4 titanium alloy powder. Then, in order to analyze the influence of different scraping methods and scraping speeds on the quality of laying, the different SLM laying processes were calculated and compared. The results of the numerical simulation study of the SLM laying powder process can be used to guide the actual SLM laying powder process and to provide basic data for the numerical simulation of the SLM molten pool dynamics based on the particle scale.

## 2 Physical modeling and numerical solution

DEM originates from molecular dynamics, which treats the entire medium as consisting of a series of discrete units of independent motion, with each element having a certain geometry (shape, size, arrangement, etc.) and physical and chemical characteristics. The motion of the unit conforms to the classical equation of motion, and the deformation and

**Fig. 7** Calculation flow



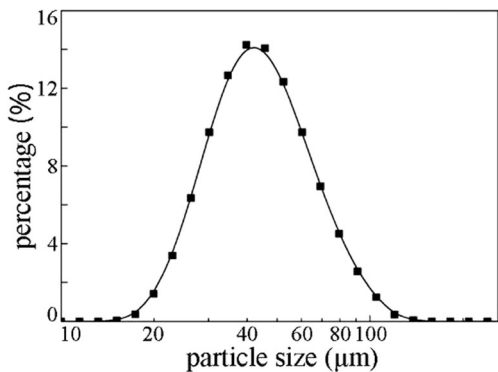


**Fig. 8** Particle size distribution of the TC4 powder [27]

evolution of the entire medium are described by the motion and position of each unit [23]. The basic principle of DEM is (1) dividing the research object into relatively independent units; (2) according to the interaction between units and Newton's law of motion, using an iterative method to determine the force and displacement of all units in each time step

and update the position of all units; and (3) by tracking and calculating the microscopic motion of each unit, obtaining the macroscopic motion law of the whole research object. The basic assumptions of DEM are that (1) the selected time step is small enough that the disturbance from other units cannot be propagated in a single time step, except for the unit that is in direct contact with the selected unit; and (2) speed and acceleration are constant over a single time step. The DEM physical model and solution flow (contact force model, collision judgment, motion equation, etc.) used in this paper will be described below.

## 2.1 Particle contact force model

The SLM laying process is a typical multi-particle action process, considering that metal particles may be slightly deformed during the collision process, and the shape of most metal particles may be considered as near-spherical. Therefore, this paper uses a soft ball model to describe the relationship between force and displacement during particle

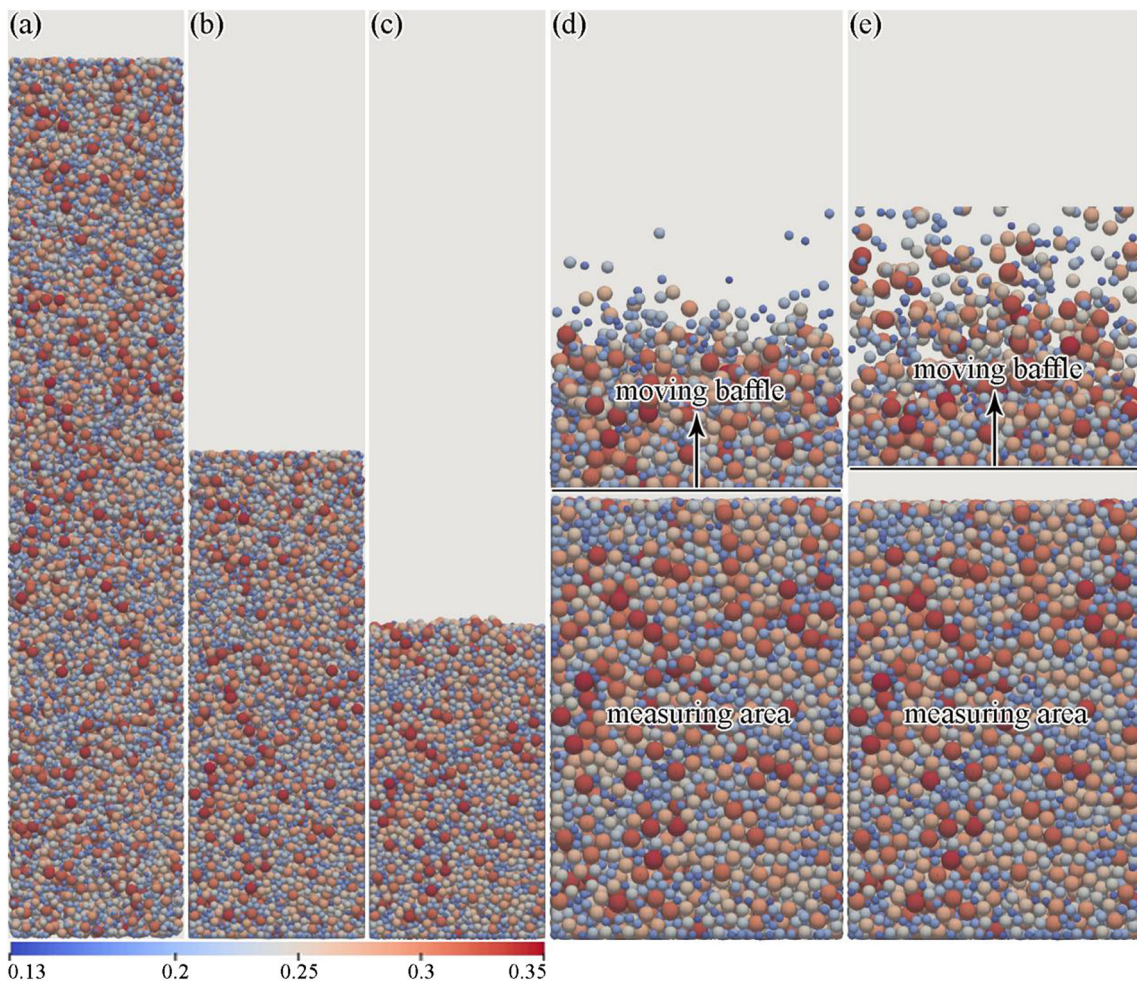


**Fig. 9** Calculation of the bulk density: **a** 0 s, initial particle cloud; **b** 2.75 s, particles dropping; **c** 6.5 s, stable particle cluster; **d** 6.75 s, baffle separating particle cluster; and **e** 7.5 s, baffle moving upwards a certain distance (unit:  $\mu\text{m}$ )

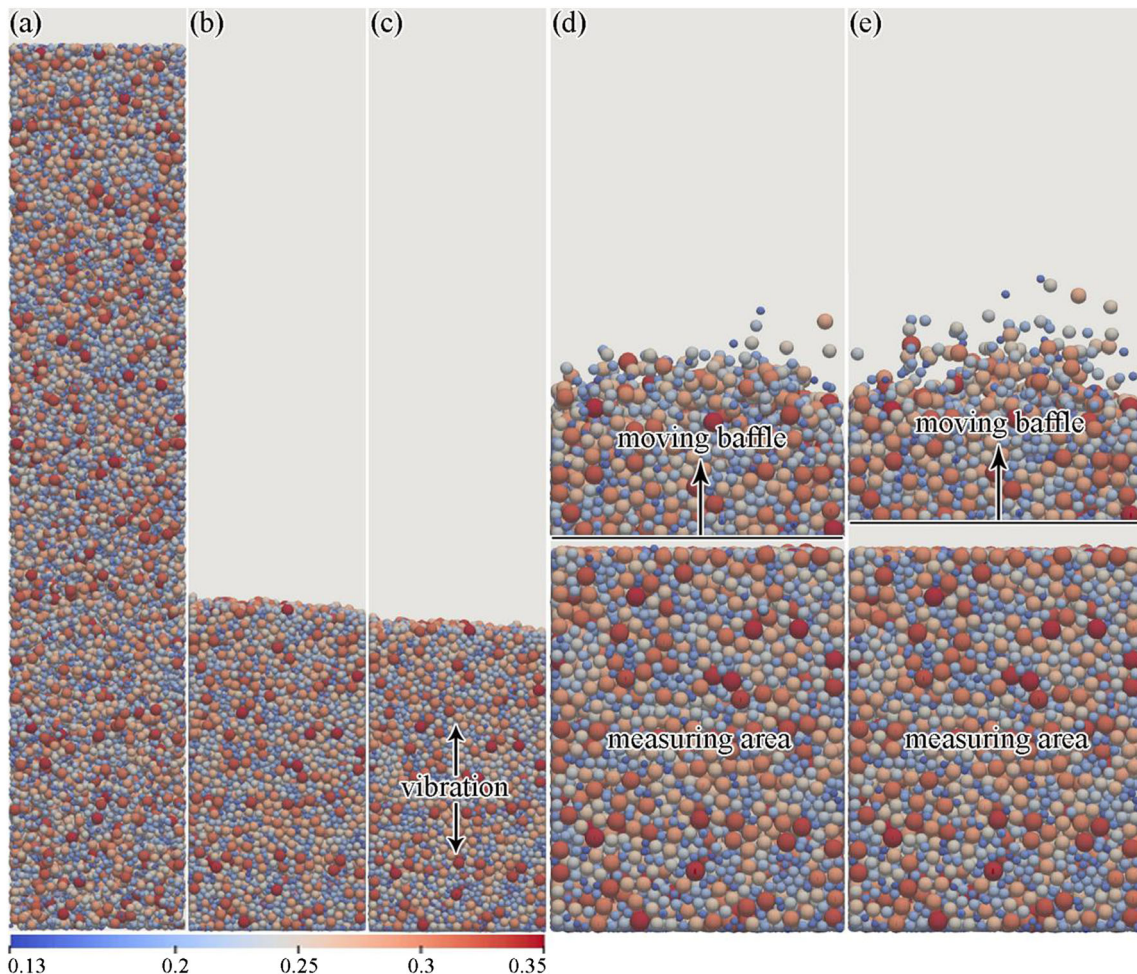


**Fig. 10** Calculation of the tap density: **a** 0 s, initial particle cloud; **b** 6.5 s, stable particle cluster; **c** 15 s, simple harmonic vibration of the container; **d** 17 s, baffle separating particle cluster; and **e** 17.5 s, baffle moving upwards a certain distance (unit:  $\mu\text{m}$ )

collision. The soft ball model can be used to simulate the simultaneous collision of two or more particles, and it was considered that the collision occurs within a certain period of time, and then the contact force between the particles was calculated according to the overlap between the balls.

The soft ball model uses the vibrational motion equation to characterize particle and particle contact, and particle and boundary contact (Fig. 4). The normal (parallel to the two-particle centerline) and tangential (vertical to the two-particle

centerline) vibrational motions during the particle contact process are decomposed, and the normal vibrational motion equation was obtained as follows:

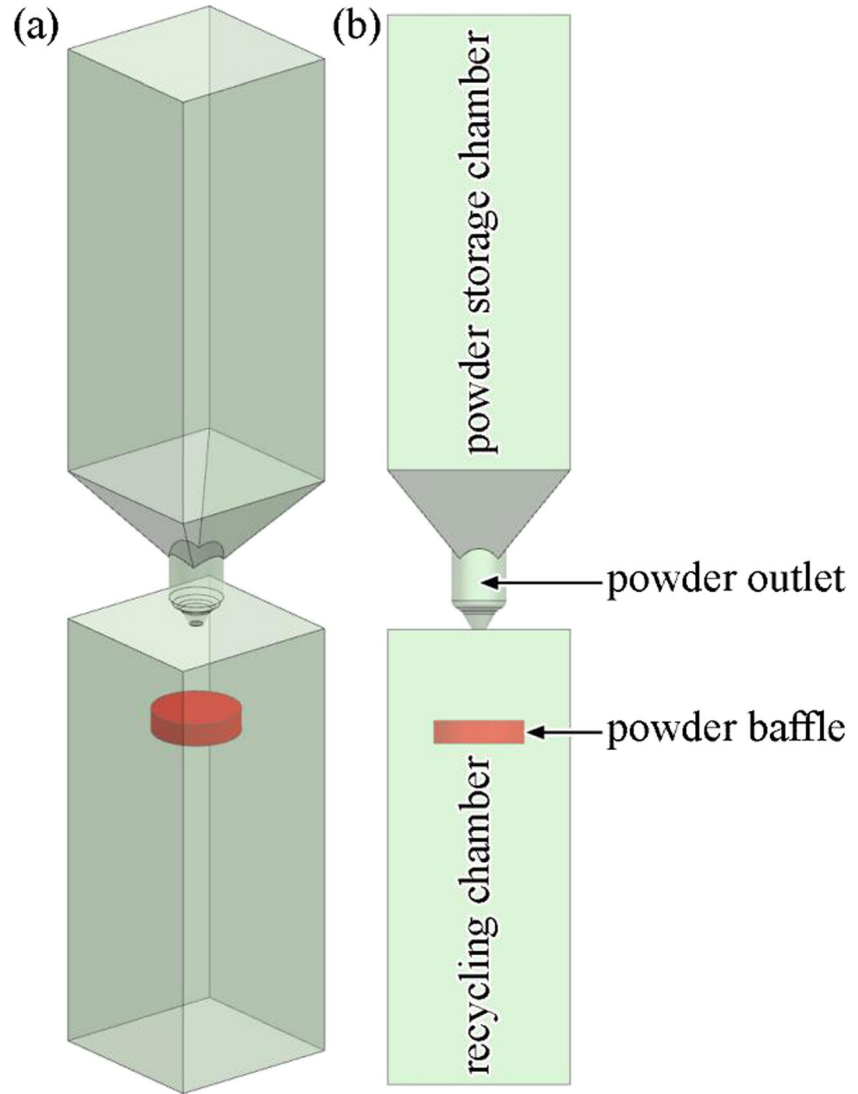
$$m_e \frac{d^2 \mathbf{u}_n}{dt^2} + D_n \frac{d\mathbf{u}_n}{dt} + E_n \mathbf{u}_n = \mathbf{F}_n \quad (1)$$

The tangential vibrational motion during the particle contact process was characterized by tangential sliding and rolling:

**Table 1** Calculation results of the bulk density and the tap density

Calculation number	Calculation of the bulk density			Calculation of the tap density		
	Number of particles	Bulk density ( $\text{kg}/\text{m}^3$ )	Average bulk density ( $\text{kg}/\text{m}^3$ )	Number of particles	Tap density ( $\text{kg}/\text{m}^3$ )	Average tap density ( $\text{kg}/\text{m}^3$ )
First calculation	18,797	2496	2494	18,075	2689	2681
Second calculation	17,581	2497		18,015	2680	
Third calculation	17,450	2488		17,250	2675	

**Fig. 11** Geometric model used for calculating the angle of repose



$$m_e \frac{d^2 \mathbf{u}_t}{dt^2} + D_t \frac{d\mathbf{u}_t}{dt} + E_t \mathbf{u}_t = \mathbf{F}_t \quad (2)$$

$$\mathbf{I}_e \frac{d^2 \theta}{dt^2} + \left( D_t \frac{d\mathbf{u}_t}{dt} + E_t \mathbf{u}_t \right) r = \mathbf{M} \quad (3)$$

The tangential sliding and rolling of the particles are affected by the friction between the particles. The sliding model can establish the limit conditions for the tangential sliding and rolling of the particles:

$$\mathbf{F}_t = \mu E_n \mathbf{u}_n \text{sgn} \left[ E_t \left( \mathbf{u}_t + \frac{d\theta}{2} \right) \right] \quad (4)$$

## 2.2 Particle collision judgment

The premise of calculating contact force is to judge which particles collide. Collision judgment algorithm has become

the subject of extensive research in the fields of robotics, computer graphics, and numerical simulation. It is roughly divided into two categories (hierarchical algorithm and flat algorithm). The idea of the hierarchical algorithm is to subdivide the space by a recursive algorithm, thereby limiting the number of elements in the first pass approximation check and ensuring that the low-level volume coincidence can only occur when the corresponding high-level volumes coincide [24]. The flat algorithm directly judges the element boundary and does not perform layered processing. Considering the complexity of the related algorithm, this paper uses the flat algorithm to judge the particle collision in the SLM laying process.

Before judging the collision of the particles, a box  $P$  was first created for the particle  $P$ , then the position and size of  $P$  were determined by the center and radius of  $P$ , so that the particle was just surrounded by the box. The necessary and sufficient condition for the collision of the two boxes is that the positions in the three directions overlap (Fig. 5):

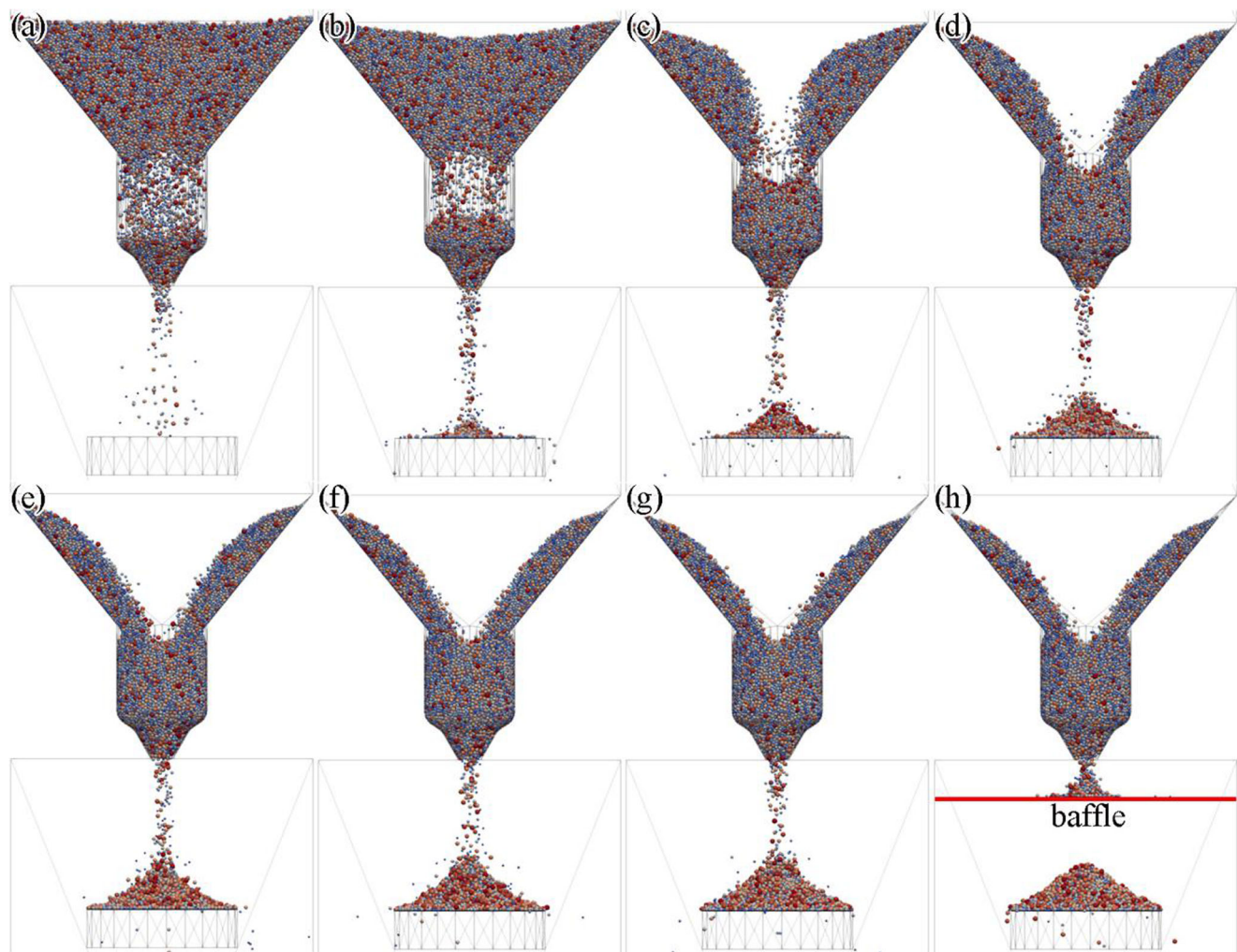


**Fig. 12** Calculation of the angle of repose: **a-f** powder free fall (the times were 5, 15, 40, 75, 100, 125 s); **g** 150 s, stable accumulation shape; and **h** 155 s, generating a baffle to obtain the final accumulation body

$$\left( \tilde{P}_i \cap \tilde{P}_j \right) \neq \Phi \Leftrightarrow \bigwedge_{w \in \{x, y, z\}} \left[ \left( \left( \tilde{P}_i^{w0}, \tilde{P}_i^{w1} \right) \cap \left( \tilde{P}_j^{w0}, \tilde{P}_j^{w1} \right) \right) \neq \Phi \right] \quad (5)$$

It should be noted that the collision of the two boxes does not mean that the two particles collide. Therefore, after the

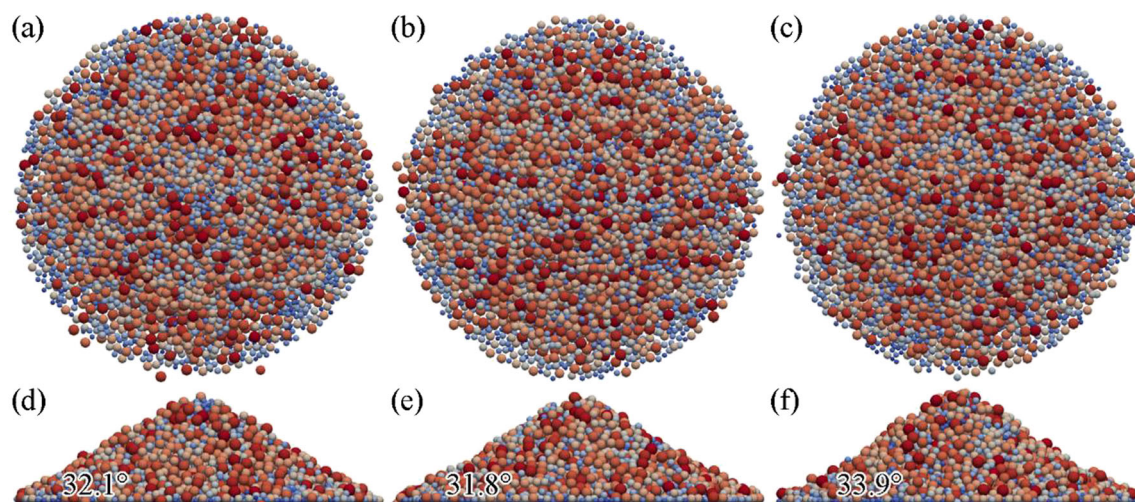


**Fig. 13** Final accumulation bodies obtained by three calculations: **a-c** top view; and **d-f** side view and the angles of repose

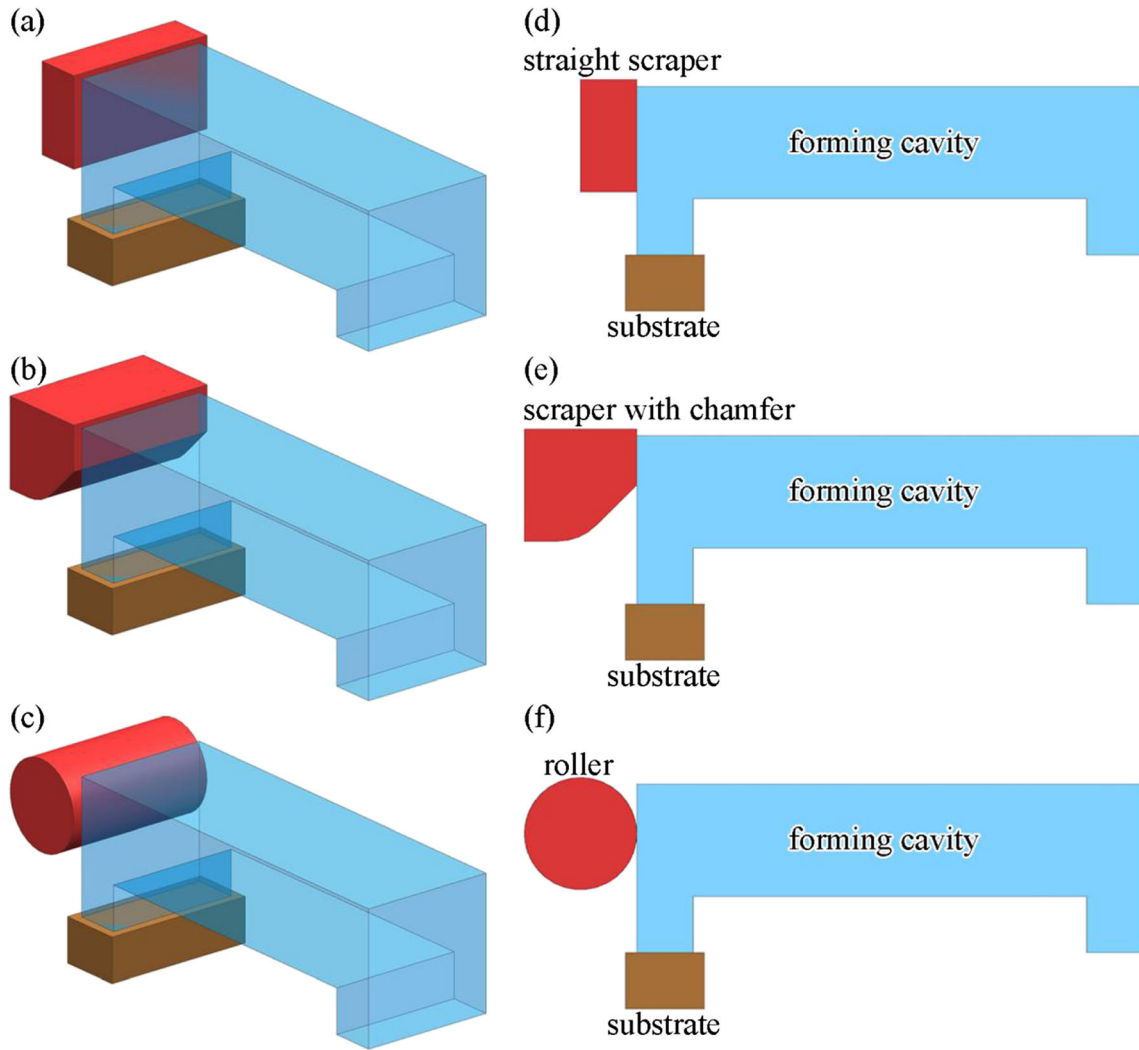


**Fig. 14** Different scraping methods: **a** straight scraper; **b** scraper with chamfer; and **c** roller

collision judgment between the boxes was completed, it was necessary to further judge the particle center, the radius, and the distance between the two particles:

$$(\tilde{P}_i \cap \tilde{P}_j) \neq \emptyset \cup L_{ij} < (r_i + r_j) \Rightarrow (P_i \cap P_j) \neq \emptyset \quad (6)$$

### 2.3 Particle motion equation

After obtaining the contact force of the particles, according to Newton's law of motion, the equation of motion of the particle  $i$  was obtained as follows:

$$m_i \ddot{\mathbf{u}}_i = \mathbf{F}_{sum} \quad (7)$$

$$\mathbf{I}_i \ddot{\theta}_i = \mathbf{M}_{sum} \quad (8)$$

Using the Euler method to simultaneously integrate both sides of Eqs. (7) and (8), the particle velocity  $(\dot{\mathbf{u}}_i)_N$  and the angular velocity  $(\dot{\theta}_i)_N$  of the next time step can be obtained:

$$(\dot{\mathbf{u}}_i)_N = (\dot{\mathbf{u}}_i)_{N-1} + \left( \frac{\mathbf{F}_{sum}}{m_i} \right)_N \Delta t \quad (9)$$

$$(\dot{\theta}_i)_N = (\dot{\theta}_i)_{N-1} + \left( \frac{\mathbf{M}_{sum}}{\mathbf{I}_i} \right)_N \Delta t \quad (10)$$

By the simultaneous integration of both sides of Eqs. (9) and (10), the updated particle displacement  $(\mathbf{u}_i)_{N+1}$  and the rotation angle  $(\theta_i)_{N+1}$  can be obtained:

$$(\mathbf{u}_i)_{N+1} = (\mathbf{u}_i)_N + (\dot{\mathbf{u}}_i)_N \Delta t \quad (11)$$

$$(\theta_i)_{N+1} = (\theta_i)_N + (\dot{\theta}_i)_N \Delta t \quad (12)$$

### 2.4 SLM laying process modeling

The prerequisite for obtaining a powder distribution that is reasonable and suitable for the SLM formation process is to establish a reasonable and complete SLM laying simulation process. Figure 6 shows a schematic diagram of the SLM

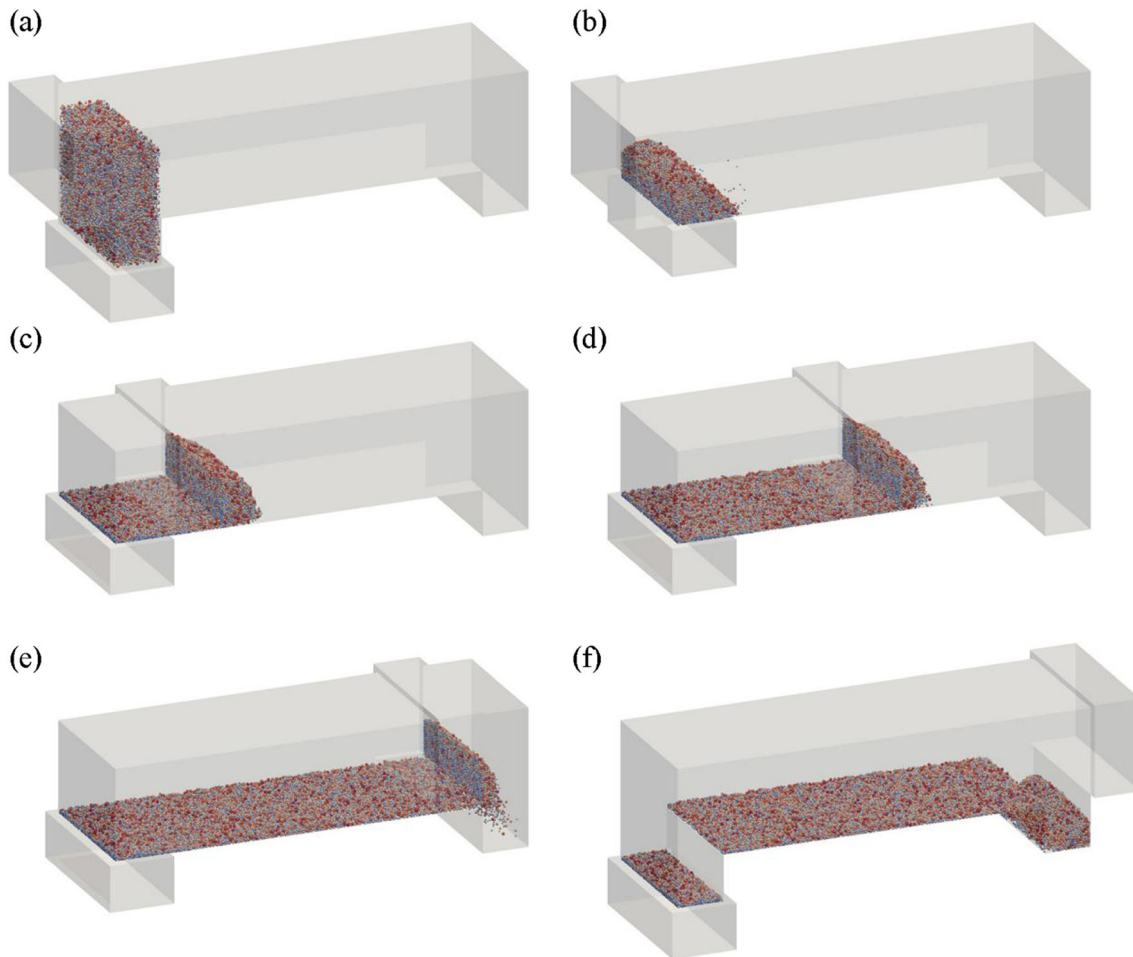


**Fig. 15** Laying powder process with the straight scraper: **a** 0 s, initial particle cloud; **b** 5.25 s, substrate pushing out powder; **c** 10 s, laying powder; **d** 15 s, laying powder; **e** 21.25 s, recycling powder; and **f** 35.25 s, finish

laying process, which consists of four steps: (1) a particle cluster is produced above the substrate, in which the initial particle positions are randomly distributed in a certain space; (2) the substrate pushes the powder cluster to the front of the roller or scraper; (3) the roller or scraper moves forward to lay powder; and (4) after the laying is finished, a powder layer with a certain thickness is obtained in the formation cavity.

## 2.5 Numerical solution of the SLM laying process

This paper is based on the open-source discrete element method code Yade [25, 26] for numerical simulation of the SLM laying process. Among them, the geometry model was imported in the form of the STL model, and the SLM laying process was implemented by custom code (including the up and down movement of the substrate, the linear motion and rotation of the roller, the linear motion of the baffle, etc.); the particle size distribution was obtained by experimental determination; metal particles were considered as elastic materials with contact friction; and the time step was calculated from the

particle radius, stiffness, and mass. Figure 7 shows a flow chart of the calculations herein.

## 3 Results and discussion

According to the above physical modeling and numerical solution process, this paper completed a numerical simulation of the SLM laying process based on Yade. In order to verify the accuracy of the SLM laying powder calculation model, the powder bulk density, tap density, and angle of repose were calculated and compared with the experimental results of the performance measurement experiment of TC4 titanium alloy powder by Liu et al. [27]. Then, in order to analyze the influence of different scraping methods and scraping speeds on the quality of laying, the different SLM laying processes were calculated and compared. In addition, the computing resources used in this paper were configured as Intel Xeon Gold 5120 CPU (32GB RAM), and the post-processing tool was ParaView.

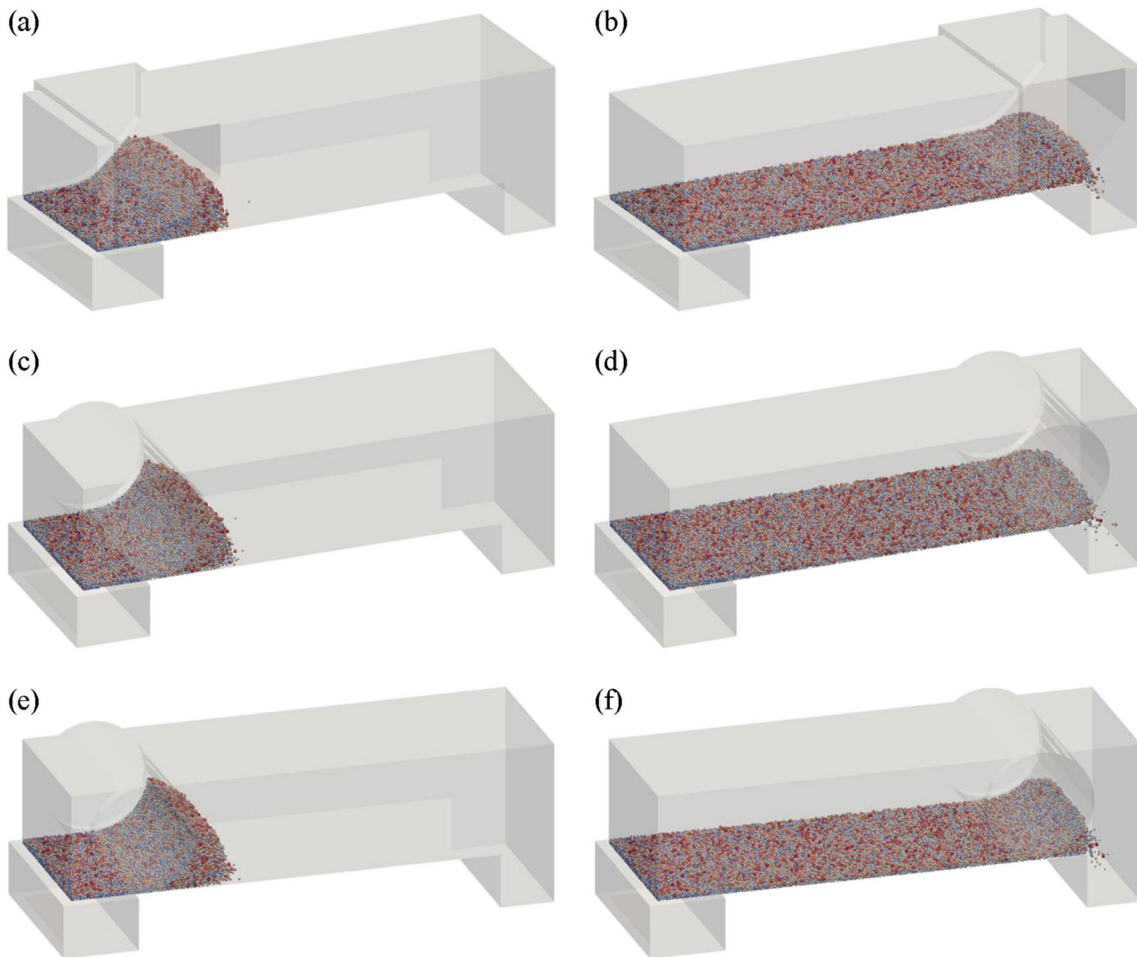


**Fig. 16** Laying powder processes with other scraping methods: **a, b** scraper with chamfer; **c, d** roller (not rotating); and **e, f** roller (rotating)

### 3.1 Powder fluidity verification

Powder fluidity is an important indicator for characterizing the process performance of powders and has a direct impact on the powder laying effect during SLM formation. In order to verify the accuracy of the laying powder model used in this paper, the fluidity of the titanium alloy powder was calculated and compared with the experimental data from the powder performance measurement. The metal powder used was a TC4 titanium alloy powder, and the corresponding particle size distribution is shown in Fig. 8. During the calculation, the particle density was set to  $4500 \text{ kg/m}^3$ , the contact friction angle was 0.5, Poisson's ratio was 0.25, and Young's modulus was 110 GPa.

First, the bulk density and tap density of the TC4 powder were calculated. The bulk density refers to the ratio of powder mass to container volume in the natural filling state, and the tap density refers to the ratio of the powder mass to container volume after proper vibration of the container. In order to ensure the calculation efficiency, the container size in this paper was set to  $1 \text{ mm} \times 1 \text{ mm} \times 5 \text{ mm}$ , and the calculation

process of the bulk density was divided into three steps (Fig. 9): (1) a particle cloud with a particle size and percentage that satisfies the distribution in Fig. 8 was randomly generated in the container; (2) the particle cloud fell freely under the action of gravity and formed a stable particle cluster; and (3) a baffle with a height of 1.5 mm was generated and moved upward by a certain distance, and the bulk density was determined by the mass of the powder under the baffle. There are two differences between the tap density calculation and the above process (Fig. 10): (1) after forming a stable particle cluster, the container was subjected to a simple harmonic vibration of 10 s (the amplitude was  $5 \mu\text{m}$  and the frequency was 50 Hz); and (2) the height of the baffle was 1.3 mm. Table 1 shows the calculation results of the bulk density and tap density. From the comparison results, the tap density was increased by 7.5% compared to the bulk density. It can be seen that container vibration has an important influence on powder filling.

Next, the angle of repose of the TC4 powder was calculated. The angle of repose refers to the maximum angle formed by the surface of the freely deposited powder and the horizontal

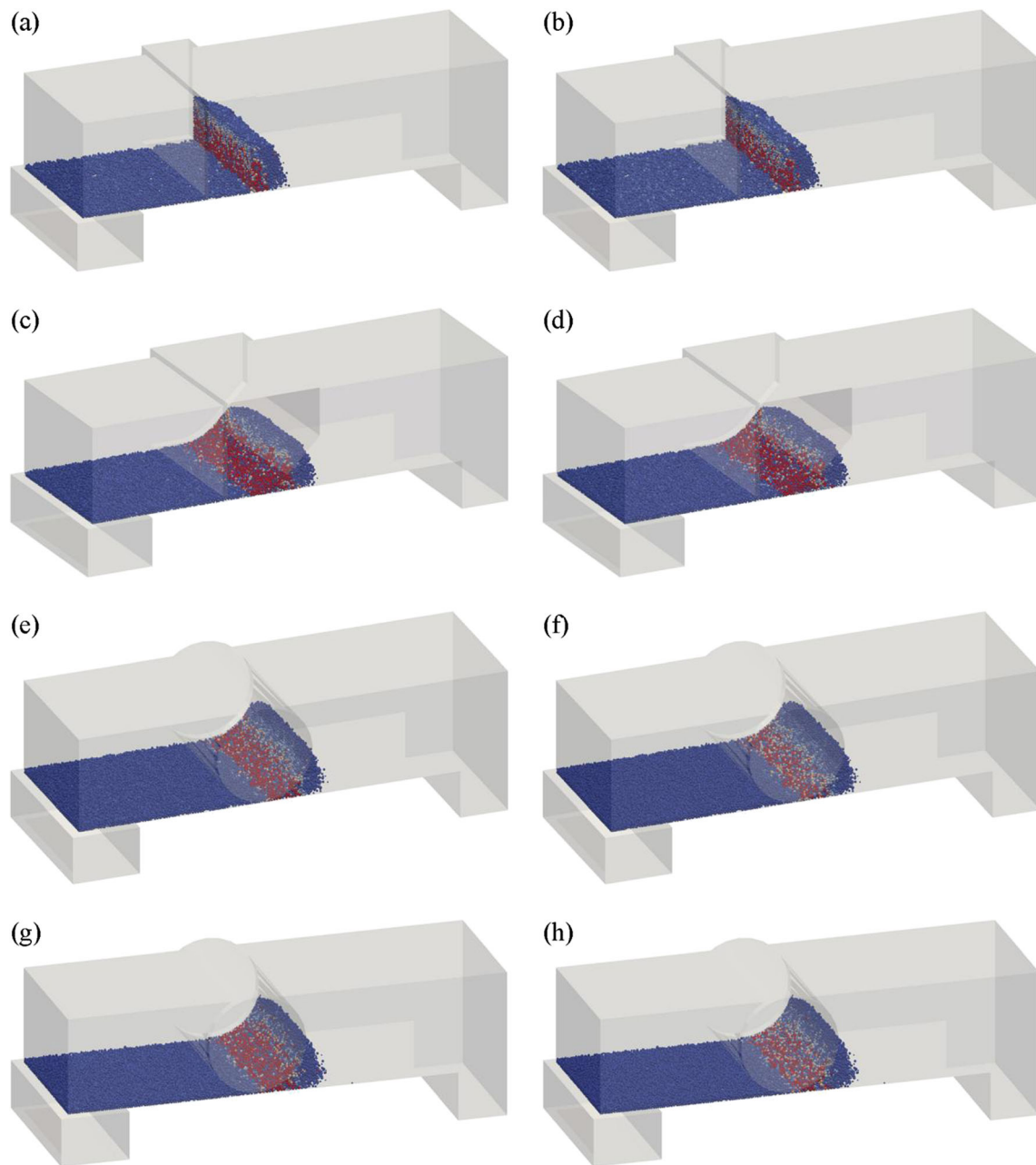


**Fig. 17** Force state of particles with different scraping methods (straight scraper, scraper with chamfer, roller (not rotating), roller (rotating)): **a, c, e, g** normal contact force; and **b, d, f, h** tangential friction (red means maximum force and blue means no force)

plane in a static equilibrium state. The geometric model used to calculate the angle of repose is shown in Fig. 11. The model consists of four parts: the powder storage chamber, the powder outlet, the powder baffle, and the recycling chamber. The diameter of the powder outlet was 0.3 mm, the diameter of the powder baffle was 2 mm, and the vertical distance between the powder outlet and the powder baffle was 2 mm. The calculation of the angle of repose was divided into three steps (Fig. 12): (1) a particle cloud was generated randomly in the powder storage chamber; (2) the particles gradually accumulated on

the baffle through the powder outlet under the action of gravity until the accumulation pattern was basically stable; and (3) a baffle was generated between the powder outlet and the baffle to obtain a final deposit. In this paper, the stacking process was calculated three times (the total number of particles were 26,848, 28,707, and 28,088), and the final deposit obtained is shown in Fig. 13. The calculated average angle of repose ( $32.6^\circ$ ) was in good agreement with the experimental data ( $33.2^\circ$ ) [27]. Therefore, the accuracy of the calculation model for the SLM paving process used in this paper was verified.

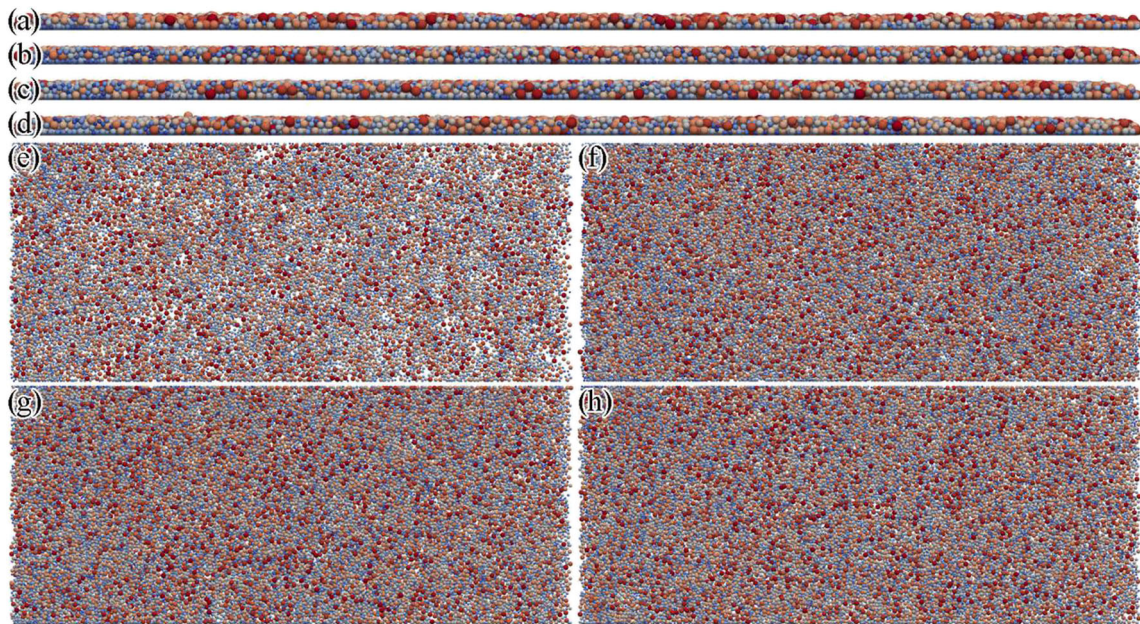


**Fig. 18** Laying distributions with different scraping methods (straight scraper, scraper with chamfer, roller (not rotating), roller (rotating)): **a-d** side view; and **e-h** top view

**Table 2** Calculation results of laying tightness with different scraping methods

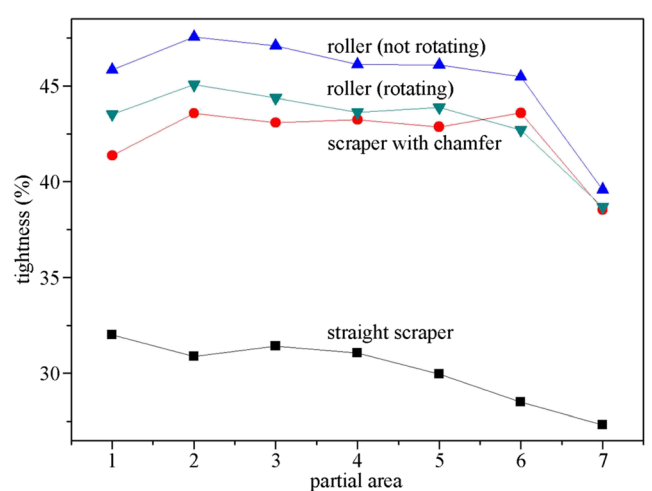
Scraping method	First calculation		Second calculation		Third calculation		Average tightness (%)
	Number of particles	Tightness (%)	Number of particles	Tightness (%)	Number of particles	Tightness (%)	
Straight scraper	25,136	30.16	26,876	30.67	27,226	30.07	30.30
Scraper with chamfer	27,355	42.33	27,449	42.11	27,681	42.19	42.21
Roller (not rotating)	27,360	45.45	27,392	45.47	27,673	45.24	45.39
Roller (rotating)	28,223	43.13	26,532	42.93	27,091	43.21	43.09

### 3.2 Effect of the scraping method on the SLM laying process

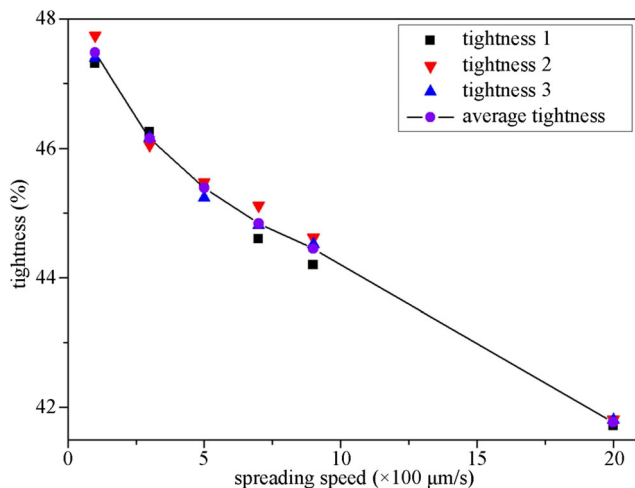
In order to analyze the influence of different scraping methods on the SLM laying process, this paper used three scrapers (straight scraper, scraper with chamfer, and roller) and four scraping methods (straight scraper laying powder, scraper with chamfer laying powder, roller (not rotating) laying powder, and roller (rotating) laying powder). The geometric model used in the calculation is shown in Fig. 14, wherein the convex portion (which is the layup region) in the formation cavity had a plane size of  $7\text{ mm} \times 3\text{ mm}$ , and the vertical distance from the lower surface of the scraper was  $120\mu\text{m}$ , and the calculation process can be found in Section 2.4. In addition, the spreading speed during the calculation of this section was  $500\mu\text{m}/\text{s}$ .

Figure 15 shows the calculation results at different times during the straight scraper laying powder process. It can be seen that a portion of the powder moved forward under the action of the straight scraper, and another portion of the powder gradually spread out in the formation cavity. After the

laying process was completed, a portion of the powder was recovered to the right cavity. Figure 16 shows the calculation results of the laying powder process in the other powder



**Fig. 19** Tightness of the local laying area with different scraping methods

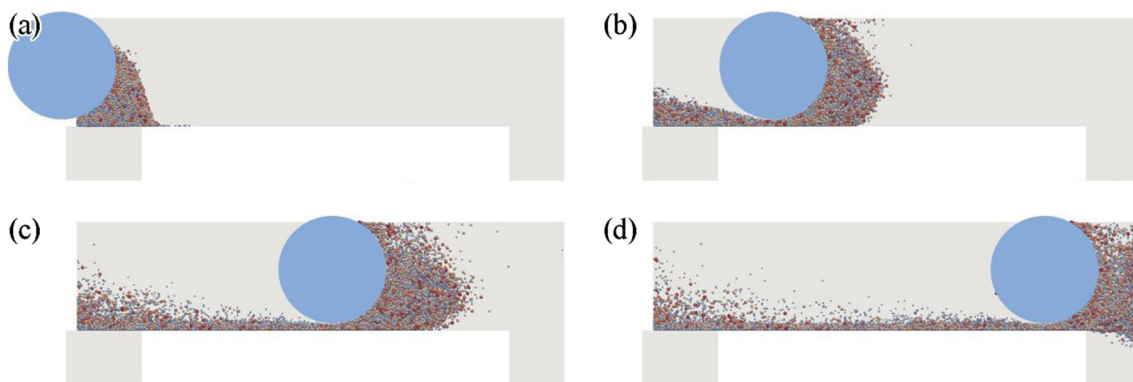
**Fig. 20** Laying tightness with different scraping speeds

scraping modes. As is apparent from the comparison results, since the contact surfaces of the two scrapers (the scraper with chamfer and the roller) with the powder were curved, the forward and laying movements of the powder were simultaneously performed.

In order to quantitatively analyze the influence of the different scraping methods on the laying process, this paper compared the stress state of the particles under different scraping modes (Fig. 17). It can be seen from the comparison results that when the straight scraper was used for laying powder, the particles in front of the scraper were subjected to the normal contact force and the tangential friction force under the combined action of gravity and the horizontal thrust of the scraper, but there was essentially no interaction between the particles below the scraper. When using the scraper with the chamfer, the roller (not rotating), and the roller (rotating) for laying, since the contact surfaces of the scrapers and the powder were curved, the particles under the scrapers were both laid and moved forward under the dual action of gravity and pressing of the scraper. Figure 18 shows the laying distributions under different scraping methods. It can be seen that, compared to other powder scraping methods, from the side view results

(Fig. 18a-d), the top surface of the layer obtained by the straight scraper was not flat, and from the top view results (Fig. 18e-h), there were obviously more voids in the layer obtained by the straight scraper. The reason for the above results is that when the powder was laid by a straight scraper, there was no interaction between the particles under the scraper, resulting in a loose particle distribution, and when other powder scraping methods were used, the particles under the scrapers were pressed so that the powder tightness was improved. From the calculation results of the tightness of the layer under different scraping methods (Table 2), it can be concluded that the tightness obtained by the straight scraper was almost 30% lower than other cases, and the tightness arrangement of the four scraping methods from high to low was roller (not rotating)>roller (rotating)>scraper with chamfer>straight scraper. The reason why the layer tightness obtained by the roller (not rotating) was higher than the roller (rotating) was because forward friction was applied to the particles during the rotation of the roller, so the particles under the roller had a stronger tendency to move forward.

The above analysis is for the overall tightness of the layer, and in actual SLM production, the uniformity of the layer distribution (the tightness of different layer areas) also has an important influence on the formation quality. Therefore, the abovementioned layer area (the convex part in the formation cavity) was artificially divided into seven equal parts along the direction of the scraping direction, and Fig. 19 shows the comparison result of the tightness of the seven partial layer areas under different scraping methods. It can be seen from the comparison results that the local area tightness obtained by the straight scraper was gradually decreasing. The reason is that the tightness in the laying process mainly depended on the accumulated pressure above the particles, and as the accumulated pressure gradually decreased, the tightness gradually decreased. When other scraping methods were adopted, the local area tightness satisfied the rule that the front and rear parts were low in tightness, while the middle part was high and uniform. The reason is that the particles in the front and rear portions were affected by the

**Fig. 21** Calculation results of the laying powder process at a scraping speed of 5 mm/s

powder storage chamber and the recycling chamber. In summary, the layer obtained by the scraping method of the roller (not rotating) had the highest tightness and most uniform powder distribution.

### 3.3 Effect of scraping speed on the SLM laying process

Next, the influence of the scraping speed on the laying process was analyzed, wherein the scraping method used a roller (not rotating), and the scraping speeds were set to 0.1, 0.3, 0.7, 0.9, and 2 mm/s. Figure 20 shows the layer tightness at different scraping speeds (calculated three times for each scraping speed), and it can be seen that as the scraping speed increased, the laying tightness tended to decrease linearly. When the powder scraping speed was too large (Fig. 21), since the impact force of the roller on the particles was too large, the particles in the layer region could not be stably maintained, and the laying could be basically considered as a failure. Therefore, in the actual SLM laying process, under the premise of ensuring production efficiency, a lower laying speed should be adopted as much as possible, which is beneficial to obtain higher layer tightness.

## 4 Conclusions

- Based on the discrete element method (particle contact force model, particle collision judgment algorithm, and particle motion equation) and the SLM laying powder process, a numerical simulation of the SLM laying powder process was carried out.
- For a performance measurement experiment of the TC4 titanium alloy powder, the powder bulk density, tap density, and angle of repose were calculated and analyzed. It was found that the tap density increased by 7.5% compared to the bulk density, and the calculated average angle of repose ( $32.6^\circ$ ) was in good agreement with the experimental data ( $33.2^\circ$ ), thus verifying the accuracy of the calculation model used for the SLM laying powder.
- The influences of different scraping methods and scraping speeds on the quality of the laying powder were calculated and analyzed. It was found that the scraping method using a roller (not rotating) obtained the highest tightness and most uniform powder distribution, and as the scraping speed increased, the laying tightness tended to decrease linearly.
- Compared with the actual laying process, there are some shortcomings, such as an insufficient number of particles used in the calculation and the ideal shape of the particle, which will be the focus of subsequent research.

**Funding information** This work was supported by the Research Platform Construction Funding of Advanced Institute of Engineering Science for Intelligent Manufacturing, Guangzhou University.

### Compliance with ethical standards

**Conflict of interest** The author declares that he has no conflict of interest.

## References

- Shipley H, McDonnell D, Culleton M, Coull R, Lupoi R, O'Donnell G (2018) Optimisation of process parameters to address fundamental challenges during selective laser melting of Ti-6Al-4V: a review. *Int J Mach Tool Manu* 128:1–20
- Yang YQ, Chen J, Song CH, Wang D, Bai YC (2018) Current status and progress on technology of selective laser melting of metal parts. *Laser Optoelectron Progress* 55(1):011401
- Gao ZJ, Zhou XL, Li JH, Zhang GJ (2018) A review: high-performance spherical metal powder preparation methods. *Therm Spray Technol* 10(3):1–9
- Xia MJ, Gu DD, Yu GQ, Dai DH, Chen HY, Shi QM (2017) Porosity evolution and its thermodynamic mechanism of randomly packed powder-bed during selective laser melting of Inconel 718 alloy. *Int J Mach Tool Manu* 116:96–106
- Cao L, Sun F, Chen T, Tang YL, Liao DM (2018) Quantitative prediction of oxide inclusion defects inside the casting and on the walls during cast-filling processes. *Int J Heat Mass Transf* 119:614–623
- Cao L, Liao DM, Sun F, Chen T (2018) Numerical simulation of cold-lap defects during casting filling process. *Int J Adv Manuf Technol* 97:2419–2430
- Xiao B, Zhang Y (2007) Marangoni and buoyancy effects on direct metal laser sintering with a moving laser beam. *Numer Heat Transf A Appl* 51(8):715–733
- Dai D, Gu DD (2014) Thermal behavior and densification mechanism during selective laser melting of copper matrix composites: simulation and experiments. *Mater Des* 55:482–491
- Michaleris P (2014) Modeling metal deposition in heat transfer analyses of additive manufacturing processes. *Finite Elem Anal Des* 86:51–60
- Lee YS, Zhang W (2015) Mesoscopic simulation of heat transfer and fluid flow in laser powder bed additive manufacturing. *Annual International Solid Freeform Fabrication Symposium* 1154–1165
- Gürtler FJ, Karg M, Leitz KH, Schmidt M (2013) Simulation of laser beam melting of steel powders using the three-dimensional volume of fluid method. *Phys Procedia* 41(1):874–879
- Khairallah SA, Anderson AT, Rubenchik A, King WE (2016) Laser powder-bed fusion additive manufacturing: physics of complex melt flow and formation mechanisms of pores, spatter, and denudation zones. *Acta Mater* 108:36–45
- Gusarov AV, Smurov I (2010) Modeling the interaction of laser radiation with powder bed at selective laser melting. *Phys Procedia* 5:381–394
- Yuan P, Gu DD (2015) Molten pool behaviour and its physical mechanism during selective laser melting of TiC/AlSi10Mg nanocomposites: simulation and experiments. *J Phys D Appl Phys* 48(3):035303
- Khairallah SA, Anderson A (2014) Mesoscopic simulation model of selective laser melting of stainless steel powder. *J Mater Process Technol* 214(11):2627–2636
- Panwisawas C, Qiu C, Anderson MJ, Sovani Y, Turner RP, Attallah MM (2017) Mesoscale modelling of selective laser melting:

- thermal fluid dynamics and microstructural evolution. *Comput Mater Sci* 126:479–490
- 17. Gürler FJ, Karg M, Dobler M, Kohl S, Tzivilsky I, Schmidt M (2014) Influence of powder distribution on process stability in laser beam melting: analysis of melt pool dynamics by numerical simulations. Annual International Solid freeform fabrication symposium 1099–1117
  - 18. Ammer R, Markl M, Ljungblad U, Körner C, Rüde U (2014) Simulating fast electron beam melting with a parallel thermal free surface lattice Boltzmann method. *Comput Math Appl* 67(2):318–330
  - 19. Panwisawas C, Qiu CL, Sovani Y, Brooks JW, Attallah MM, Basoalto HC (2015) On the role of thermal fluid dynamics into the evolution of porosity during selective laser melting. *Scr Mater* 105:14–17
  - 20. Markl M, Körner C (2016) Multiscale modeling of powder bed-based additive manufacturing. *Annu Rev Mater Res* 46:93–123
  - 21. Parteli EJR, Pöschel T (2016) Particle-based simulation of powder application in additive manufacturing. *Powder Technol* 288:96–102
  - 22. Yan W, Ge W, Qian Y, Lin S, Zhou B, Liu WK (2017) Multi-physics modeling of single/multiple-track defect mechanisms in electron beam selective melting. *Acta Mater* 134:324–333
  - 23. Cundall PA, Strack ODL (1979) A discrete numerical model for granular assemblies. *Geotechnique* 29(1):47–65
  - 24. Hubbard PM (1996) Approximating polyhedra with spheres for time-critical collision detection. *ACM Trans Graph* 15(3):179–210
  - 25. Alaba A, Lambert S, Nicot F, Chareyre B (2015) Relation between microstructure and loading applied by a granular flow to a rigid wall using DEM modeling. *Granul Matter* 17(5):603–616
  - 26. Yuan C, Chareyre B (2017) A pore-scale method for hydromechanical coupling in deformable granular media. *Comput Method Appl Mech Eng* 318:1066–1079
  - 27. Liu BY (2018) Cyclic aging behavior of TC4 powder and the influence on properties of components built by SLM. Master Thesis, Shenyang Aerospace University

**Publisher's note** Springer Nature remains neutral with regard to jurisdictional claims in published maps and institutional affiliations.